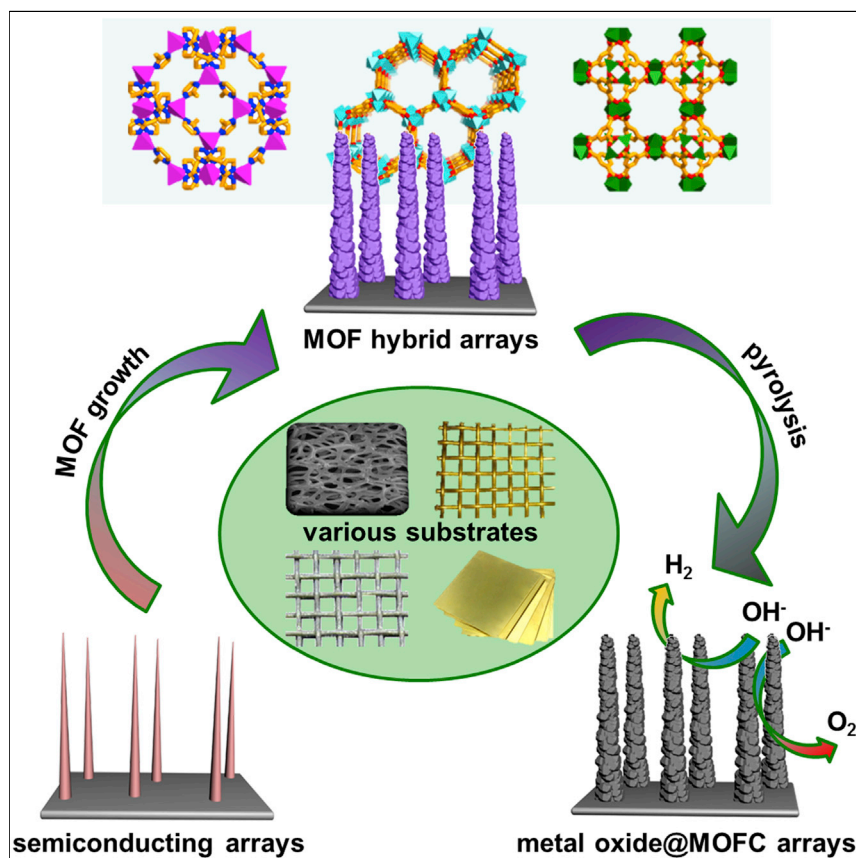


## Article

# Template-Directed Growth of Well-Aligned MOF Arrays and Derived Self-Supporting Electrodes for Water Splitting



Traditional metal-organic framework (MOF) nanocrystals are not optimized for applications, and their conversion to self-supporting MOF superstructures is highly desired. We develop a general strategy for the fabrication of various MOF hybrid arrays on diverse substrates. Furthermore, the MOF arrays with derived carbon-based composites with well-aligned hierarchical morphology and self-supporting structure can be applied directly to both anodes and cathodes for water splitting. This approach opens a new avenue for the assembly of MOF-based nanocrystals for broad applications.

Guorui Cai, Wang Zhang, Long Jiao, Shu-Hong Yu, Hai-Long Jiang

shyu@ustc.edu.cn (S.-H.Y.)  
jianglab@ustc.edu.cn (H.-L.J.)

## HIGHLIGHTS

The template-directed strategy is general, facile, and controllable

A rational design guides the assembly of MOF nanocrystals on well-aligned templates

A series of MOF-based hybrid arrays can be fabricated on various substrates

The self-supporting composites can be used directly as electrodes for water splitting



Cai et al., Chem 2, 791–802  
June 8, 2017 © 2017 Elsevier Inc.  
<http://dx.doi.org/10.1016/j.chempr.2017.04.016>

## Article

# Template-Directed Growth of Well-Aligned MOF Arrays and Derived Self-Supporting Electrodes for Water Splitting

Guorui Cai,<sup>1,2</sup> Wang Zhang,<sup>1,2</sup> Long Jiao,<sup>1</sup> Shu-Hong Yu,<sup>1,\*</sup> and Hai-Long Jiang<sup>1,3,\*</sup>

## SUMMARY

The conversion of traditional metal-organic framework (MOF) nanocrystals to self-supporting and well-aligned MOF superstructures is highly desired for diverse functional applications but remains a significant challenge. In this work, we develop a versatile strategy for the controllable synthesis of three-dimensional MOF hybrid arrays by utilizing semiconducting nanostructures as self-sacrificing templates. Typically, different MOF nanorod or nanowall arrays on various substrates have been successfully fabricated. Particularly, MOF-hybrid-array-derived carbon-based composites with well-aligned hierarchical morphology and self-supporting structure can be directly applied to both anodes and cathodes for water splitting. They exhibit excellent electrocatalytic performance and are superior to the pristine semiconducting arrays, as well as other MOF-based counterparts. This work provides a strategy for the rational assembly of well-aligned MOF arrays on various substrates, which could serve as a promising platform for diverse applications.

## INTRODUCTION

As a relatively new class of porous crystalline materials, metal-organic frameworks (MOFs) have aroused widespread interest because of their high surface area, intriguing structures, and multifunctional properties.<sup>1–7</sup> Given the crystalline, tailored, and periodic porous texture of MOFs, their derived porous carbon composites (MOFCs), with high porosity and surface area as well as uniform active heteroatom doping, exhibit broad applications in energy conversion and storage, especially in electrocatalysis, such as the oxygen reduction reaction (ORR), hydrogen evolution reaction (HER), oxygen evolution reaction (OER), etc.<sup>8–28</sup> Currently, most of the reported MOFCs have been obtained via direct pyrolysis of MOF crystals,<sup>8–15</sup> which seems straightforward and facile but is actually not optimized for electrocatalysis. The MOF particles are prone to aggregate during pyrolysis at high temperature, which renders the resultant MOFC agglomerates unfavorable for electron conductivity and the transport of reactants and products in electrocatalytic reactions. To address this issue, considering the advantages of MOF superstructures,<sup>29–36</sup> we have recently demonstrated that the fabrication of one-dimensional (1D) MOF superstructures improves the electrocatalytic performance by simultaneously preventing particle aggregation and maintaining an oriented arrangement of MOFCs.<sup>37</sup> Despite this, particle agglomeration sometimes occurs as a result of the intrinsic nature of small particles. The subsequent fabrication procedure for the electrode, coating the electrocatalyst onto a conductive substrate (such as carbon cloth, Ni foam, etc.), is elaborate and time consuming and requires additional polymeric binders. Moreover, the mechanical stability and electric contact of the catalyst layer

## The Bigger Picture

To address increasing environmental and energy concerns, it is highly desirable to generate clean-energy products via a sustainable route. Hydrogen production from water splitting is one of the most promising technologies for meeting this target. The key to realizing industrialization is the design of efficient catalysts as electrode materials. Metal-organic frameworks (MOFs) provide an ideal platform for designing promising catalysts because of their porosity and diversity. However, most MOF materials are powders, which seem straightforward and facile but are actually not optimal for practical application. To optimize performance, we demonstrate a general strategy for the preparation of various MOFs and derived carbon-based hybrid arrays that serve as efficient self-supporting electrodes in both oxygen evolution reactions and hydrogen evolution reactions for water splitting. In addition, this template-directed strategy provides a design guide for the assembly of MOF nanocrystals on various well-aligned substrates.

are usually problematic, particularly in HERs and OERs, because the fast bursting of H<sub>2</sub> or O<sub>2</sub> bubbles readily makes the coated MOFCs peel off from the electrodes.

To meet this challenge, direct growth of MOF arrays throughout a conductive matrix is highly desirable, especially with a three-dimensional (3D) meso- or macroporous structure. The ensuing pyrolysis then leads to MOFC arrays inside the matrix for electrocatalysis with several intrinsic advantages:<sup>38–45</sup> (1) the undesired issues (such as MOFC aggregation, elaborate electrode preparation, peeling of MOFCs from substrates, etc.) mentioned above can be avoided because the MOFC arrays can act directly as electrodes for catalytic reactions; (2) the oriented and close arrangement of the MOFCs inherited from the MOF arrays improves the electrical conductivity, increases the electrochemically active surface area, and accelerates the timely release of gas bubbles; (3) the close and strong binding of MOFCs with the underlying conductive support guarantees fast electron transportation between them and ultrahigh structural stability of the electrodes; and (4) the large pores inside the matrix promote penetration and diffusion of the electrolyte. To our knowledge, although there have been very few reports on the growth of MOFs with 1D nanowire arrays onto a planar 2D substrate,<sup>46,47</sup> the rational fabrication of various well-aligned MOFs on different metal oxides and hydroxides and/or their derived hybrid arrays onto various (including 2D and 3D) conductive matrices remains a significant challenge, and there have been no reports so far.

In view of the fact that metal oxide and hydroxide arrays on diverse substrates have been reported,<sup>48–52</sup> it is possible to grow metal oxides and hydroxides as self-sacrificing templates onto a 3D matrix and then convert them to MOF arrays. Using this idea, we have successfully developed a versatile approach to fabricating metal oxide@MOF or metal hydroxide@MOF hybrid arrays in this work. Different metal oxides and hydroxides (such as CoO, NiO, and Cu(OH)<sub>2</sub>; Figure S1) in well-aligned architecture can be grown successfully onto various substrates (Ni foam, Cu mesh, Fe mesh, or Cu foil; Figure S2); then the reaction with related organic ligands turns the metal oxides and hydroxides into corresponding MOFs, such as ZIF-67 (Co(mim)<sub>2</sub>, Hmim = 2-methylimidazole), MOF-74 (Ni<sub>2</sub>(dhtp) or Co<sub>2</sub>(dhtp), H<sub>4</sub>dhtp = 2,5-dihydroxyterephthalic acid), and HKUST-1 (Cu<sub>3</sub>(btc)<sub>2</sub>, H<sub>3</sub>btc = 1,3,5-benzenetricarboxylic acid) (Figure S3) nanorod and nanowall arrays.<sup>53–57</sup> Taking the resultant ZIF-67 on Ni foam (denoted as Ni@CoO@ZIF-67) as an example, the hybrid arrays can be further converted to CoO@MOFC hybrid with well-retained array architecture and high surface area via a facile pyrolysis (Figure 1), which can be used directly as a self-supporting electrode. Results have manifested that the CoO@MOFC hybrid array exhibits better activity and durability toward OERs and HERs than do its corresponding counterparts. The excellent electrocatalytic performances are mainly attributed to the readily accessible active species, expedited electron transportation, and electrolyte penetration, as well as convenient bursting of the gas bubbles from the electrodes, as a result of the hierarchical pores of 3D arrays and synergistic advantages between the metal oxide core and the MOFC shell.

## RESULTS AND DISCUSSION

### Synthesis and Characterization of Well-Aligned CoO@ZIF-67 Hybrid Arrays on Ni Foam: Ni@CoO@ZIF-67

With relatively high electron conductivity, high macroporosity, and low cost, Ni foam was first chosen as a substrate for the preparation of metal oxide and/or hydroxide arrays (Figure S4). Typically, the Ni foam was immersed in Co<sup>2+</sup> solution and underwent hydrothermal reactions for the preparation of CoO nanowire arrays on it (Ni@CoO). The CoO nanowire arrays were grown vertically on Ni foam in the usual

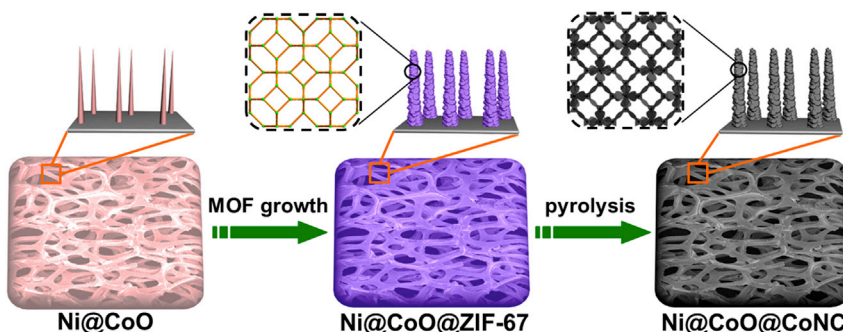
<sup>1</sup>Hefei National Laboratory for Physical Sciences at the Microscale, CAS Key Laboratory of Soft Matter Chemistry, Collaborative Innovation Center of Suzhou Nano Science and Technology, Department of Chemistry, University of Science and Technology of China, Hefei, Anhui 230026, China

<sup>2</sup>These authors contributed equally

<sup>3</sup>Lead Contact

\*Correspondence: shyu@ustc.edu.cn (S.-H.Y.), jianglab@ustc.edu.cn (H.-L.J.)

<http://dx.doi.org/10.1016/j.chempr.2017.04.016>

**Figure 1. Schematic Illustration**

Schematic illustration showing the fabrication of metal oxide@MOF hybrid arrays and their derived metal oxide@MOFC arrays on the 3D conductive matrix based on metal oxide as the MOF (ZIF-67) as a representative precursor. See also Figures S1 and S2.

way (Figures 1 and S5) and were then chosen as self-sacrificial precursors or templates to provide  $\text{Co}^{2+}$  ions and a skeleton for the growth of ZIF-67, for which they were dissolved with the assistance of solvent and ligand. This process endowed hybrid arrays with a uniform rod-like nanostructure (Figures 2A and S6), indicating that the morphology was well preserved with local corrosion of the metal oxide arrays. Close observation by transmission electron microscopy (TEM) revealed the formation of a core-shell heterostructure in a rod-like morphology with significantly different contrast between core and shell (Figure 2B). Energy-dispersive X-ray spectroscopy (EDS) analysis of the core-shell structure showed a much higher Co signal in the center than in the shell layer (Figure S7), indicating that part of the  $\text{CoO}$  nanowire was left in the interior along with the outer MOF shell formed. The powder X-ray diffraction (XRD) pattern of the resultant product matched well with that of the simulated ZIF-67 phase, manifesting the formation of pure ZIF-67 (Figure 2C). The  $\text{N}_2$  sorption curves and pore-size distributions suggested the presence of microporosity from ZIF-67 and the meso- or macroporosity from 3D Ni foam (Figures 2D and S8). All these results unambiguously demonstrate the successful fabrication of hierarchically porous  $\text{Ni@CoO@ZIF-67}$  hybrid arrays.

#### The Growth Mechanism of Well-Aligned MOF Hybrid Arrays

To clarify the growth mechanism, we further investigated time-dependent reactions to track the process of conversion (Figure S9). In the initial stage (1 min), some small ZIF-67 nanoparticles ( $\sim 40$  nm) were deposited on the surface of  $\text{CoO}$  nanorods ( $\sim 100$  nm; Figures S9B and S9F). When the reaction time was prolonged to 1 hr, more nanoparticles piled up to generate a continuous layer (Figures S9C and S9G). Upon reaction for 12 hr, the thickness of the MOF shell increased to  $\sim 140$  nm, and the diameter of the  $\text{CoO}$  core decreased to  $\sim 47$  nm (Figures S9D and S9H). As the reaction proceeded, the ZIF-67 shell became thicker as a result of the corrosion of the  $\text{CoO}$  core. This phenomenon reveals that the ligand was able to penetrate the pores of ZIF-67 and react with the inner  $\text{CoO}$  species, as well as deprotonate to produce  $\text{H}^+$ , which led to the dissolution of  $\text{CoO}$  to  $\text{Co}^{2+}$ . The  $\text{Co}^{2+}$  ions diffused outward to react with the ligand at the outer surface of the ZIF-67 layer for continuous growth. ZIF-67 grew much more slowly when the MOF shell became thick, possibly as a result of the diffusion limitation. The thickness of ZIF-67 almost reached a maximum value and stopped increasing after reaction for  $\sim 12$  hr.

The above process strongly suggests a competing mechanism whereby the dissolution of metal oxide at the solid-liquid interface and the precipitation of ZIF-67

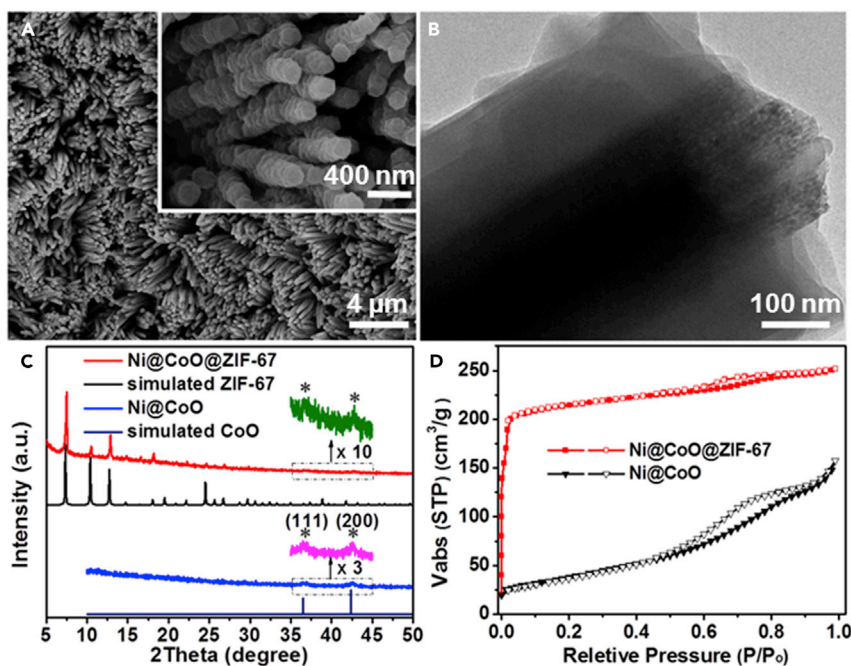


**Figure 2. SEM and TEM Images, Powder XRD Patterns, and N<sub>2</sub> Sorption Isotherms**

(A and B) SEM (A) and TEM (B) images of as-prepared Ni@CoO@ZIF-67 arrays. Inset: enlarged SEM image. See also Figure S6. Scale bars: 4  $\mu$ m (A), 400 nm (inset of A), and 100 nm (B).

(C) Powder XRD patterns of experimental Ni@CoO, Ni@CoO@ZIF-67, simulated CoO, and simulated ZIF-67. The asterisks indicate the (111) and (200) peaks of CoO species.

(D) N<sub>2</sub> sorption isotherms of Ni@CoO and Ni@CoO@ZIF-67. See also Figure S8.

particles by the coordination between metal ions and 2-methylimidazole (2-MeIM) linkers occur at the same time. Therefore, the balance between the dissolution and coordination rate is crucial for the formation of well-defined CoO@ZIF-67 nano-rod arrays on Ni foam. Typically, when ethanol is used as the solvent, the corrosion rate is too slow to release enough Co<sup>2+</sup> for the formation of ZIF-67 (Figure S10A). In contrast, the speed of dissolution in water is very fast, leading to the preferred self-nucleation in solution rather than the expected epitaxial growth on the surface of CoO nanorods (Figures S10B and S10C). Hence, the appropriate solvent is necessary for the successful preparation of CoO@ZIF-67 nanostructures, and a mixed solvent involving ethanol and water was adopted to control CoO dissolution. 2-MeIM plays a dual role as both an etching reagent to release Co<sup>2+</sup> ions and a coordinator with Co<sup>2+</sup> ions to form ZIF-67 during the synthesis. In addition, when CoO is replaced with Co<sub>3</sub>O<sub>4</sub>, the synthesis of the Ni@Co<sub>3</sub>O<sub>4</sub>@ZIF-67 heterostructure is unsuccessful (Figure S10D), inferring that not only proper reaction conditions but also an appropriate metal precursor are critical for controllable MOF growth.

### The Generality and Versatility of the Template-Directed Strategy for MOF-Based Hybrid Arrays

Given that various metal oxide and even hydroxide arrays (NiO, ZnO, ZnCo<sub>2</sub>O<sub>4</sub>, Cu(OH)<sub>2</sub>, etc.) can be easily grown on different substrates (Ti foil, Cu foil, conductive glass, etc.),<sup>48–52</sup> it is expected that the above self-sacrificing template strategy can be extended to the growth of a variety of MOF arrays on different substrates, which would be highly desirable for diverse applications. To demonstrate this, in addition to the above Ni foam, we used other substrates such as Cu mesh, Fe mesh, and Cu foil to successfully grow ZIF-67 nanorod arrays on all of them by following similar

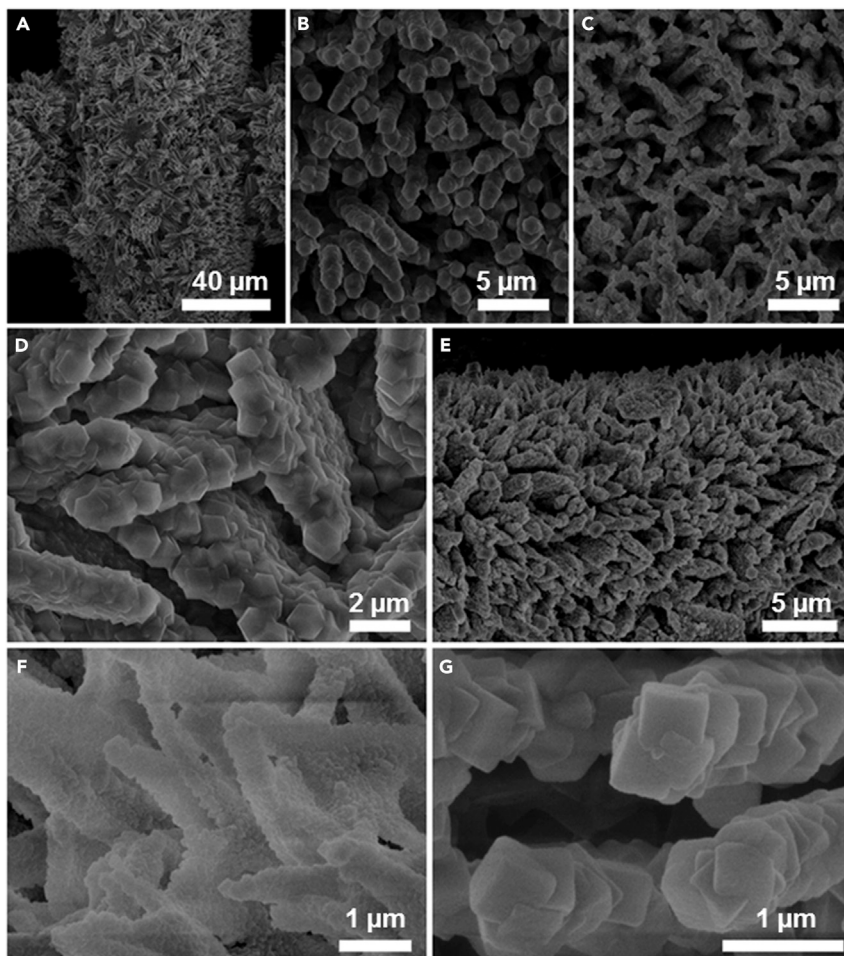


**Figure 3. SEM Images of Different MOF Hybrid Arrays on Various Substrates**

SEM images of CoO@ZIF-67 nanorod arrays on various substrates: Cu mesh (A), Fe mesh (B), and Cu foil (C). Also shown are SEM images of ZIF-67 nanowall arrays on Ni foam (D), CoO@Co-MOF-74 nanorod arrays on Ni foam (E), NiO@Ni-MOF-74 nanorod arrays on Ni foam (F), and Cu(OH)<sub>2</sub>@HKUST-1 nanorod arrays on Cu mesh (G). Scale bars: 40 μm (A), 5 μm (B, C, and E), 2 μm (D), and 1 μm (F and G). See also Figures S11–S22.

synthetic procedures (Figures 3A–3C and S11–S13). Interestingly, changing the shape of pristine precursor arrays can readily adjust the shape of MOF arrays, for example, CoO@ZIF-67 nanorods from CoO nanowires and CoO@ZIF-67 nanowalls from CoO nanowalls (Figures 3D, S14, and S15). Moreover, on the basis of the same metal oxide arrays, different MOF arrays can be fabricated by the introduction of corresponding organic ligands. Taking CoO nanowire arrays on Ni foam as an example, not only was Ni@CoO@ZIF-67 obtained with the use of 2-methylimidazole as indicated above, but Ni@CoO@Co-MOF-74 was also achieved by the introduction of the ligand 2,5-dihydroxyterephthalic acid (Figures 3E and S16). More importantly, diverse metal oxide and even hydroxide arrays can be grown onto the substrates, which guarantees the successful growth of a variety of metal oxide@MOF or metal hydroxide@MOF hybrid arrays, for example, CoO arrays for CoO@ZIF-67 arrays, NiO arrays for NiO@Ni-MOF-74 arrays (Figures 3F, S17, and S18), and Cu(OH)<sub>2</sub> arrays for Cu(OH)<sub>2</sub>@HKUST-1 arrays (Figures 3G and S19–S22). All of these results unambiguously demonstrate the generality and versatility of the current synthetic strategy for MOF-based hybrid arrays.

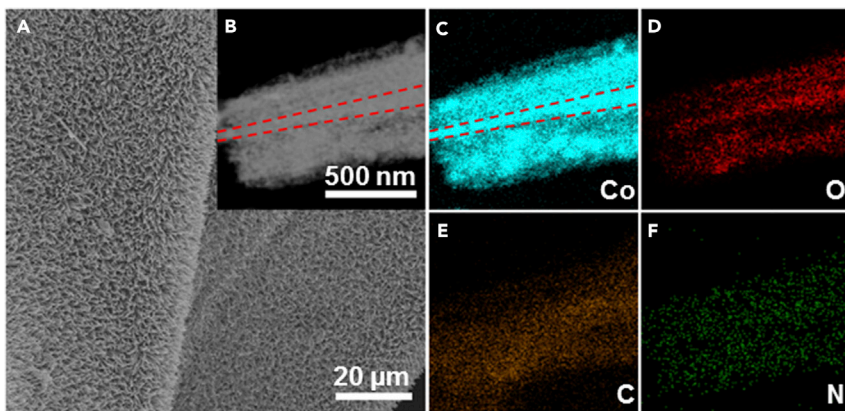


**Figure 4. SEM and HAADF-STEM Images and Elemental Mappings**

SEM (A) and HAADF-STEM (B) images of Ni@CoO@CoNC with corresponding Co, O, C, and N elemental mappings (C–F). Scale bars: 20  $\mu\text{m}$  (A) and 500 nm (B). See also Figure S23.

### Preparation and Characterization of MOFC Hybrid Arrays

Considering that MOFs have been well demonstrated to be excellent templates and precursors for metal or metal oxide and porous carbon nanocomposites,<sup>8–15</sup> the metal oxide and hydroxide@MOFs arrays obtained could be thermally converted to their corresponding 3D hybrid metal oxide@porous carbon arrays on the substrate, which would be an ideal electrode directly applicable in electrocatalysis; particularly, the MOF-derived porous carbon involved would not only improve the electrical conductivity but also facilitate the accessibility of active sites, thus enhancing the catalytic performance. As an example of the feasibility of this, the as-prepared Ni@CoO@ZIF-67 was facilely converted to Ni@CoO@Co/N-doped porous carbon arrays (denoted as Ni@CoO@CoNC) by pyrolysis in a  $\text{N}_2$  atmosphere. Scanning electron microscopy (SEM) images of Ni@CoO@CoNC revealed that the structure of the original Ni@CoO@ZIF-67 nanorod arrays was almost preserved except for slight shrinkage of the nanorod (Figures 4A and S23), which is commonly observed in MOF-pyrolyzed derivatives.<sup>8–23</sup> The powder XRD profile of Ni@CoO@CoNC suggests that the shell was composed of crystalline Co/N-doped porous carbon, in agreement with a previous report on ZIF-67-derived nanocomposites at low pyrolysis temperatures (Figure S24).<sup>58</sup> The high-angle annular dark-field scanning transmission electron microscopy (HAADF-STEM) image shows a dense core coated with a loose shell in each nanorod, suggesting a core-shell structure (Figure 4B), in which the core of CoO nanorod (highlighted with a red dashed line in Figure 4C) looks brighter than the shell because of the much higher Co signal. The corresponding elemental mappings demonstrate that the CoO@CoNC is mainly composed of Co, O, C, and N, which are well dispersed throughout the nanorods (Figures 4C–4F).

### The HER and OER Performances of Ni@CoO@CoNC

The HER performance of Ni@CoO@CoNC was first investigated in a typical three-electrode configuration. It reached an overpotential of 190 mV at a current density of 10 mA/cm<sup>2</sup> with a Tafel slope of 98 mV/dec, which is superior to that of CoO@CoNC powder deposited on Ni foam (Ni/CoO@CoNC) and pristine Ni@CoO (Figures 5A and 5B). In addition, the Ni@CoO@CoNC electrode showed significantly enhanced OER activity to afford an overpotential of 309 mV at a current density of 10 mA/cm<sup>2</sup> and a Tafel slope of 53 mV/dec, much better than those of Ni/CoO@CoNC, Ni@CoO and even IrO<sub>2</sub>, the state-of-the-art OER catalyst (Figures 5C and 5D).<sup>59</sup> For preparation of the Ni/CoO@CoNC sample, CoO@CoNC on Ni

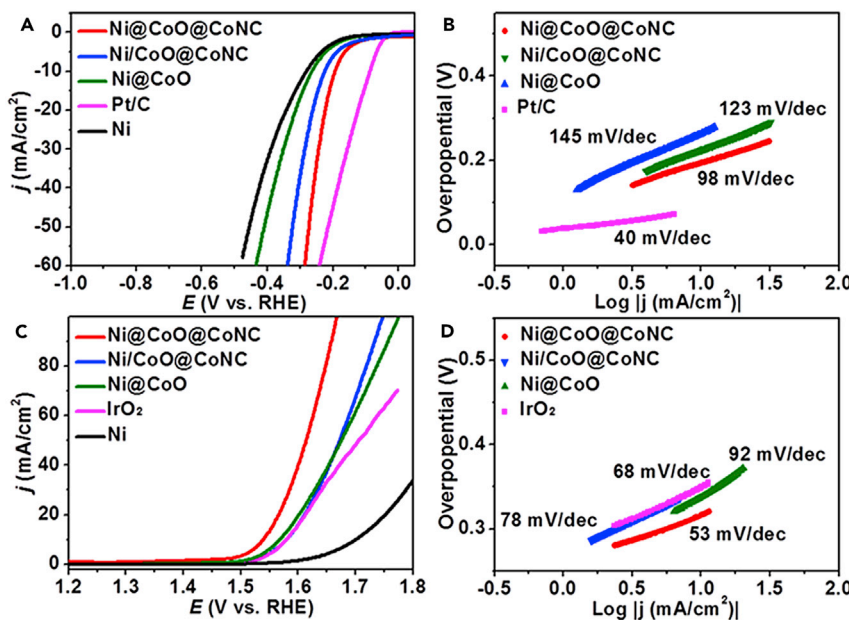


**Figure 5. Polarization Curves and Tafel Plots**

(A and B) HER polarization curves (A) and corresponding Tafel plots (B) of Ni@CoO@CoNC, Ni/CoO@CoNC, Ni@CoO, Ni foam, and Pt/C.

(C and D) OER polarization curves (C) and corresponding Tafel plots (D) of Ni@CoO@CoNC, Ni/CoO@CoNC, Ni@CoO, Ni foam, and IrO<sub>2</sub>.

foam was coated with additional polymeric binder. Therefore, the electrode had the same active part of CoO@CoNC as Ni@CoO@CoNC, but its structure was disorganized and unstable. The better HER and OER performances of Ni@CoO@CoNC than of Ni/CoO@CoNC clearly suggest the advantage of a well-organized and self-supporting structure. To gain further insight into the effect of the MOF-derived CoNC shell on the electrochemical process, we examined the OER performance of Ni@CoO@CoNC hybrid arrays derived from the Ni@Co@ZIF-67 precursors with different MOF thicknesses and found that the MOF thickness had an important influence on OER activity (Figure S25). Furthermore, the electrical impedance spectrum was also obtained (Figure S26). Ni@CoO@CoNC had less internal resistance and more efficient electronic transmission than Ni@CoO, which implies a synergistic effect of the core-shell structure. In addition, chronoamperometry tests showed that Ni@CoO@CoNC remained highly active even after 20 hr, and its polarization curves after 3,000 cycles showed a negligible drop during HER and OER processes (Figures S27 and S28).

### Conclusion

In summary, we have developed a versatile strategy for the synthesis of metal oxide@MOF or metal hydroxide@MOF hybrid arrays on various substrates by using metal oxide and hydroxide nanostructured arrays as self-sacrificing templates, in which the substrate, metal oxide or hydroxide, MOF, and even the shape (nanorod or nanowall) of the array can be altered. Remarkably, by simple pyrolysis, the obtained MOF-based hybrid arrays can be further transformed into metal oxide@MOF-derived porous carbon hybrid arrays with well-aligned hierarchical and self-supporting structure. The latter can be used directly as an efficient electrode for both HER and OER and exhibit much higher activity, more favorable kinetics, and better durability than the corresponding counterparts (Ni@metal oxide

or MOF-derived nanocomposite without a self-supporting structure). The excellent electrocatalytic performance can be ascribed to the porous nanoarray electrode configuration, *in situ* carbon incorporation, increased exposure and accessibility of active sites, accelerated release of gas bubbles, robust structure, and great mass and charge transport. It is expected that this self-sacrificing template strategy will provide new opportunities for the rational assembly of well-aligned 3D MOF nanocrystals on substrates, which would serve as important platforms for device applications, especially in energy storage and conversion.

## EXPERIMENTAL PROCEDURES

### Materials

All chemicals were from commercial suppliers without further purification unless otherwise mentioned. See [Supplemental Experimental Procedures](#) for more details.

### Preparation of Ni@CoO

The CoO nanowire array was synthesized on Ni foam by a hydrothermal reaction. In detail, 582 mg of cobalt nitrate hexahydrate, 600 mg of urea, and 296 mg of ammonium fluoride were dissolved in 36 mL of deionized water. The homogeneous solution obtained was transferred into a Teflon-lined stainless steel autoclave with a piece of clean nickel foam (4 × 3.5 cm) immersed into the reaction solution. The autoclave was sealed and maintained at 120°C for 10 hr and then cooled down to room temperature. The array sample was collected and rinsed with distilled water several times and then directly annealed at 350°C in N<sub>2</sub> gas for 1 hr at a heating rate of 2°C/min.

### Preparation of Ni@CoO@ZIF-67

Typically, 1.64 g of 2-methylimidazole was dissolved in 5 mL of deionized water and 5 mL of absolute ethanol, and then a piece of Ni@CoO foam obtained as above was immersed into the reaction solution, which was maintained at room temperature for 12 hr. The array sample was collected and rinsed with absolute ethanol several times and then dried in an oven at 85°C for 12 hr to give Ni@CoO@ZIF-67.

### Preparation of CoO Nanowire Arrays on Cu Mesh, Fe Mesh, or Cu Foil

The Cu mesh, Fe mesh, or Cu foil (4 × 3.5 cm) was first washed with concentrated HCl and then deionized water for the removal of the oxide layer. Other procedures followed the preparation of Ni@CoO nanowire arrays described above, except that the Ni foam was replaced with Cu mesh, Fe mesh, or Cu foil.

### Preparation of CoO@ZIF-67 Nanorod Arrays on Cu Mesh, Fe Mesh, or Cu Foil: Cu Mesh@CoO@ZIF-67, Fe Mesh@CoO@ZIF-67, or Cu Foil@CoO@ZIF-67

The same procedure as for the preparation of Ni@CoO@ZIF-67 described above was used, except that Ni@CoO was replaced with Cu mesh@CoO, Fe mesh@CoO, or Cu foil@CoO.

### Preparation of Ni@CoO Nanowall Arrays

The CoO nanowall arrays were deposited on Ni foam by a technique similar to the preparation of Ni@CoO nanowire arrays described above, except that the hydrothermal reaction was maintained at 100°C for 6 hr.

### Preparation of Ni@CoO@ZIF-67 Nanowall Arrays

The same procedure as for the preparation of Ni@CoO@ZIF-67 described above was used, except that the Ni@CoO nanowire arrays were replaced with Ni@CoO nanowall arrays.

### Preparation of CoO@Co-MOF-74 Nanorod Arrays on Ni Foam: Ni@CoO@Co-MOF-74

Typically, 2,5-dihydroxyterephthalic acid (35 mg) was dissolved in a mixed solvent of 10 mL of *N,N*-dimethylformamide, 0.5 mL of absolute ethanol, and 0.5 mL of deionized water. Then a piece of Ni@CoO foam was immersed into the reaction solution and maintained at 120°C for 1 hr. The array sample was collected and rinsed with absolute ethanol several times and then dried in an oven at 85°C for 12 hr to give Ni@CoO@Co-MOF-74.

### Preparation of Ni@NiO

Typically, 1.16 g of nickel nitrate hexahydrate and 200 mg of potassium persulfate were dissolved in 35 mL of deionized water. The homogeneous solution obtained was further transferred into a Teflon-lined stainless steel autoclave with a piece of clean nickel foam (4 × 3.5 cm) immersed into the reaction solution, which was sealed and maintained at 150°C for 10 hr and then cooled down to room temperature. The array sample was collected and rinsed with distilled water several times and then directly annealed at 400°C in N<sub>2</sub> gas for 1 hr at a heating rate of 2°C/min.

### Preparation of Ni@NiO@Ni-MOF-74

Typically, 2,5-dihydroxyterephthalic acid (20 mg) was dissolved in a mixed solution containing 5 mL of *N,N*-dimethylformamide, 0.5 mL of absolute ethanol, and 0.5 mL of deionized water. Then a piece of Ni@NiO foam was immersed into the reaction solution and maintained at 130°C for 1 hr. The array sample was collected and rinsed with absolute ethanol several times and then dried at 85°C in an oven for 12 hr to give Ni@NiO@Ni-MOF-74.

### Preparation of Cu Mesh@Cu(OH)<sub>2</sub>

Typically, 1 g of sodium hydroxide and 228 mg of ammonium persulfate were dissolved in 10 mL of deionized water. Then a piece of Cu mesh (3 × 4.5 cm) was immersed into the reaction solution (which was maintained at room temperature for 20 min), washed with distilled water several times, and then dried in an oven at 120°C for 24 hr.

### Preparation of Cu Mesh@Cu(OH)<sub>2</sub>@HKUST-1

Typically, 10 mg of 1,3,5-benzene tricarboxylic acid and 100 mg of polyvinylpyrrolidone were dissolved in 2.5 mL of deionized water and 2.5 mL of *N,N*-dimethylformamide. Then a piece of Cu mesh@Cu(OH)<sub>2</sub> foam was immersed into the reaction solution, which was maintained at room temperature for 10 min. The array sample was collected and rinsed with absolute ethanol several times and then dried in an oven at 85°C for 12 hr.

### Preparation of Cu Foil@Cu(OH)<sub>2</sub>

The same procedures as for the preparation of Cu mesh@Cu(OH)<sub>2</sub> were followed, except that the Cu mesh was replaced with Cu foil.

### Preparation of Cu Foil@Cu(OH)<sub>2</sub>@HKUST-1

The same procedures as for the preparation of Cu mesh@Cu(OH)<sub>2</sub>@HKUST-1 were followed, except that the Cu mesh@Cu(OH)<sub>2</sub> was replaced with Cu foil@Cu(OH)<sub>2</sub>.

### Preparation of CoO@MOFC Hybrid Arrays on Ni Foam: Ni@CoO@MOFC

Ni@CoO@ZIF-67 was selected as an example to afford CoO@Co/N-doped porous carbon arrays on Ni foam (Ni@CoO@CoNC). Typically, the as-prepared

Ni@CoO@ZIF-67 arrays were put into a ceramic boat and transferred into a temperature-programmed furnace in a N<sub>2</sub> flow and then heated to 350°C for 3 hr at a heating rate of 2°C/min. The sample was then further pyrolyzed at 500°C for 2 hr.

#### Preparation of CoO Powders

CoO powders were prepared according to the procedure for Ni@CoO but without Ni foam.

#### Preparation of CoO@ZIF-67 Powders

CoO@ZIF-67 powders were obtained with the procedures described above for Ni@CoO@ZIF-67, except the Ni@CoO arrays were replaced with CoO powders.

#### Preparation of CoO@CoNC Powders

CoO@CoNC powders were prepared according to the procedures for Ni@CoO@CoNC described above, except the Ni@CoO@ZIF-67 arrays were replaced with CoO@ZIF-67 powders.

#### Electrochemical Measurement

The HER and OER tests were performed with a CHI 760E electrochemical analyzer (CH Instruments). All electrochemical measurements were conducted in a standard three-electrode system with a Pt foil as the counter electrode, Ag/AgCl as the reference electrode, and the self-supporting arrays grown on Ni foam (1 × 1 cm, mass loading ~4 mg/cm<sup>2</sup>) as the working electrode. Before the electrochemical measurements were conducted, 1 M KOH solution was purged with N<sub>2</sub> (HER tests) or O<sub>2</sub> (OER tests) for 30 min. After several cyclic voltammetry tests with a scan rate of 50 mV/s to get stable curves, linear sweep voltammetry for OER and HER was performed at a scanning rate of 0.5 mV/s. The stability investigations were operated at constant overpotentials (309 mV for OER and 190 mV for HER). The current density was normalized to the geometrical area, and potentials versus Ag/AgCl were converted to versus RHE (reversible hydrogen electrode) according to the Nernst equation ( $E_{\text{RHE}} = E_{\text{Ag/AgCl}} + 0.059 \times \text{pH} + 0.197$ ). The Tafel slope was calculated according to the following formula  $\eta = b \log(j/j_0)$ , where  $\eta$  is the overpotential,  $b$  is the Tafel slope,  $j$  is the current density, and  $j_0$  is the exchange current density. Ni foam, Ni@CoO, Pt/C (20 wt %), IrO<sub>2</sub>, and Ni/CoO@CoNC (4 mg of CoO@CoNC powder was dispersed in 1 mL of ethanol containing 20 μL of 5 wt % Nafion and then sonicated for 30 min; finally, the catalyst ink was coated on Ni foam) were also tested for comparison. All the tests were carried out at room temperature and presented without iR compensation.

#### Characterization

Powder XRD patterns were recorded on a Japan Rigaku DMax- $\gamma$ A rotation anode X-ray diffractometer equipped with graphite monochromatized Cu K $\alpha$  radiation ( $\lambda = 1.54 \text{ \AA}$ ). SEM was carried out with a field emission scanning electron microanalyzer (Zeiss Supra 40 scanning electron microscope) operating at an acceleration voltage of 5 kV. TEM, EDS, HAADF-STEM, and elemental mapping were acquired on JEOL-2010, JEOL-2100F, and JEOL ARM-200F electron microscopes with an electron acceleration energy of 200 kV. Nitrogen sorption measurements were conducted with automatic volumetric adsorption equipment (Micrometrics ASAP, 2020) at 77 K. Before the nitrogen adsorption and desorption measurements, the samples were dried overnight at 150°C under vacuum.

## SUPPLEMENTAL INFORMATION

Supplemental Information includes Supplemental Experimental Procedures and 28 figures and can be found with this article online at <http://dx.doi.org/10.1016/j.chempr.2017.04.016>.

## AUTHOR CONTRIBUTIONS

G.C. and W.Z. contributed equally to this work. H.-L.J. and S.-H.Y. conceived the idea and supervised the project. G.C. and W.Z. designed and performed the experiments and collected the data. L.J. analyzed the electrocatalytic data. H.-L.J. and G.C. co-wrote the paper. All authors discussed the results and commented on the manuscript.

## ACKNOWLEDGMENTS

This work was supported by the National Natural Science Foundation of China (21371162, 21673213, 21521001, 21431006, and 91227103), the Ministry of Science and Technology of China (2014CB931800 and 2013CB933900), the Chinese Academy of Sciences (KJZD-EW-M01-1), and the Recruitment Program of Global Youth Experts.

Received: March 15, 2017

Revised: April 7, 2017

Accepted: April 26, 2017

Published: June 8, 2017

## REFERENCES AND NOTES

1. Zhou, H.-C., Long, J.R., and Yaghi, O.M. (2012). Introduction to metal-organic frameworks. *Chem. Rev.* 112, 673–674.
2. Li, B., Wen, H.-M., Cui, Y., Zhou, W., Qian, G., and Chen, B. (2016). Emerging multifunctional metal-organic framework materials. *Adv. Mater.* 28, 8819–8860.
3. Wang, H., Zhu, Q.-L., Zou, R., and Xu, Q. (2017). Metal-organic frameworks for energy applications. *Chem* 2, 52–80.
4. Zhu, Q.-L., and Xu, Q. (2014). Metal-organic framework composites. *Chem. Soc. Rev.* 43, 5468–5512.
5. He, L., Liu, Y., Liu, J., Xiong, Y., Zheng, J., Liu, Y., and Tang, Z. (2013). Core-shell noble-metal@metal-organic-framework nanoparticles with highly selective sensing property. *Angew. Chem. Int. Ed.* 52, 3741–3745.
6. Zhao, M., Yuan, K., Wang, Y., Li, G., Guo, J., Gu, L., Hu, W., Zhao, H., and Tang, Z. (2016). Metal-organic frameworks as selectivity regulators for hydrogenation reactions. *Nature* 539, 76–80.
7. Lu, Q., Zhao, M., Chen, J., Chen, B., Tan, C., Zhang, X., Huang, Y., Yang, J., Cao, F., Yu, Y., et al. (2016). In situ synthesis of metal sulfide nanoparticles based on 2D metal-organic framework nanosheets. *Small* 12, 4669–4674.
8. Ma, S., Goenaga, G.A., Call, A.V., and Liu, D.-J. (2011). Cobalt imidazolate framework as precursor for oxygen reduction reaction electrocatalysts. *Chem. Eur. J.* 17, 2063–2067.
9. Su, P., Xiao, H., Zhao, J., Yao, Y., Shao, Z., Li, C., and Yang, Q. (2013). Nitrogen-doped carbon nanotubes derived from Zn-Fe-ZIF nanospheres and their application as efficient oxygen reduction electrocatalysts with in situ generated iron species. *Chem. Sci.* 4, 2941–2946.
10. Zhang, P., Sun, F., Xiang, Z., Shen, Z., Yun, J., and Cao, D. (2014). ZIF-derived in situ nitrogen-doped porous carbons as efficient metal-free electrocatalysts for oxygen reduction reaction. *Energy Environ. Sci.* 7, 442–450.
11. Zhao, D., Shui, J.-L., Grabstanowicz, L.R., Chen, C., Commet, S.M., Xu, T., Lu, J., and Liu, D.-J. (2014). Highly efficient non-precious metal electrocatalysts prepared from one-pot synthesized zeolitic imidazolate frameworks. *Adv. Mater.* 26, 1093–1097.
12. Zhao, S., Yin, H., Du, L., He, L., Zhao, K., Chang, L., Yin, G., Zhao, H., Liu, S., and Tang, Z. (2014). Carbonized nanoscale metal-organic frameworks as high performance catalyst for oxygen reduction reaction. *ACS Nano* 8, 12660–12668.
13. Lin, Q., Bu, X., Kong, A., Mao, C., Zhao, X., Bu, F., and Feng, P. (2015). New heterometallic zirconium metallocporphyrin frameworks and their heteroatom-activated high-surface-area carbon derivatives. *J. Am. Chem. Soc.* 137, 2235–2238.
14. Xia, W., Mahmood, A., Zou, R., and Xu, Q. (2015). Metal-organic frameworks and their derived nanostructures for electrochemical energy storage and conversion. *Energy Environ. Sci.* 8, 1837–1866.
15. Cao, F., Zhao, M., Yu, Y., Chen, B., Huang, Y., Yang, J., Cao, X., Lu, Q., Zhang, X., Zhang, Z., et al. (2016). Synthesis of two-dimensional  $\text{CoS}_{1.097}$ /nitrogen-doped carbon nanocomposites using metal-organic framework nanosheets as precursors for supercapacitor application. *J. Am. Chem. Soc.* 138, 6924–6927.
16. Liu, B., Shioyama, H., Akita, T., and Xu, Q. (2008). Metal-organic framework as a template for porous carbon synthesis. *J. Am. Chem. Soc.* 130, 5390–5391.
17. Jiang, H.-L., Liu, B., Lan, Y.-Q., Kuratani, K., Akita, T., Shioyama, H., Zong, F., and Xu, Q. (2011). From metal-organic framework to nanoporous carbon: toward a very high surface area and hydrogen uptake. *J. Am. Chem. Soc.* 133, 11854–11857.
18. Almasoudi, A., and Mokaya, R. (2012). Preparation and hydrogen storage capacity of templated and activated carbons nanocast from commercially available zeolitic imidazolate framework. *J. Mater. Chem.* 22, 146–152.
19. Hu, M., Reboul, J., Furukawa, S., Torad, N.L., Ji, Q., Srinivasu, P., Ariga, K., Kitagawa, S., and Yamauchi, Y. (2012). Direct carbonization of Al-based porous coordination polymer for synthesis of nanoporous carbon. *J. Am. Chem. Soc.* 134, 2864–2867.
20. Srinivas, G., Krungleviciute, V., Guo, Z.-X., and Yildirim, T. (2014). Exceptional  $\text{CO}_2$  capture in a hierarchically porous carbon with simultaneous high surface area and pore volume. *Energy Environ. Sci.* 7, 335–342.
21. Zheng, F., Yang, Y., and Chen, Q. (2014). High lithium anodic performance of highly nitrogen-doped porous carbon prepared from a metal-organic framework. *Nat. Commun.* 5, 5261.
22. Chen, Y.-Z., Wang, C., Wu, Z.-Y., Xiong, Y., Xu, Q., Yu, S.-H., and Jiang, H.-L. (2015). From

- bimetallic metal-organic framework to porous carbon: high surface area and multicomponent active dopants for excellent electrocatalysis. *Adv. Mater.* 27, 5010–5016.
23. Tang, Y.-J., Gao, M.-R., Liu, C.-H., Li, S.-L., Jiang, H.-L., Lan, Y.-Q., Han, M., and Yu, S.-H. (2015). Porous molybdenum-based hybrid catalysts for highly efficient hydrogen evolution. *Angew. Chem. Int. Ed.* 54, 12928–12932.
24. Zhao, S., Wang, Y., Dong, J., He, C.-T., Yin, H., An, P., Zhao, K., Zhang, X., Gao, C., Zhang, L., et al. (2016). Ultrathin metal-organic framework nanosheets for electrocatalytic oxygen evolution. *Nat. Energy* 1, 16184.
25. Yin, H., Zhao, S., Zhao, K., Muqsit, A., Tang, H., Chang, L., Zhao, H., Gao, Y., and Tang, Z. (2015). Ultrathin platinum nanowires grown on single-layered nickel hydroxide with high hydrogen evolution activity. *Nat. Commun.* 6, 6430.
26. Zheng, Y., Jiao, Y., Zhu, Y., Li, L.H., Han, Y., Chen, Y., Jaroniec, M., and Qiao, S.-Z. (2016). High electrocatalytic hydrogen evolution activity of an anomalous ruthenium catalyst. *J. Am. Chem. Soc.* 138, 16174–16181.
27. Cao, X., Tan, C., Zhang, X., Zhao, W., and Zhang, H. (2016). Solution-processed two-dimensional metal dichalcogenide-based nanomaterials for energy storage and conversion. *Adv. Mater.* 28, 6167–6196.
28. Zhu, Y.P., Guo, C., Zheng, Y., and Qiao, S.-Z. (2017). Surface and interface engineering of noble-metal-free electrocatalysts for efficient energy conversion processes. *Acc. Chem. Res.* 50, 915–923.
29. Ameloot, R., Vermoortele, F., Vanhove, W., Roeckaers, M.B.J., Sels, B.F., and De Vos, D.E. (2011). Interfacial synthesis of hollow metal-organic framework capsules demonstrating selective permeability. *Nat. Chem.* 3, 382–387.
30. Reboul, J., Furukawa, S., Horike, N., Tsotsalas, M., Hirai, K., Uehara, H., Kondo, M., Louvain, N., Sakata, O., and Kitagawa, S. (2012). Mesoscopic architectures of porous coordination polymers fabricated by pseudomorphic replication. *Nat. Mater.* 11, 717–723.
31. Yanai, N., Sindoro, M., Yan, J., and Granick, S. (2012). Electric field-induced assembly of monodisperse polyhedral metal-organic framework crystals. *J. Am. Chem. Soc.* 135, 34–37.
32. Sindoro, M., Yanai, N., Jee, A.Y., and Granick, S. (2014). Colloidal-sized metal-organic frameworks: synthesis and applications. *Acc. Chem. Res.* 47, 459–469.
33. Carné-Sánchez, A., Imaz, I., Cano-Sarabia, M., and Maspoch, D. (2013). A spray-drying strategy for synthesis of nanoscale metal-organic frameworks and their assembly into hollow superstructures. *Nat. Chem.* 5, 203–211.
34. Cao, X., Zheng, B., Rui, X., Shi, W., Yan, Q., and Zhang, H. (2014). Metal oxide-coated three-dimensional graphene prepared by the use of metal-organic frameworks as precursors. *Angew. Chem. Int. Ed.* 53, 1404–1409.
35. Yao, M.-S., Tang, W.-X., Wang, G.-E., Nath, B., and Xu, G. (2016). MOF thin film-coated metal oxide nanowire array: significantly improved chemiresistor sensor performance. *Adv. Mater.* 28, 5229–5234.
36. Li, Z., Shao, M., Zhou, L., Zhang, R., Zhang, C., Wei, M., Evans, D.G., and Duan, X. (2016). Directed growth of metal-organic frameworks and their derived carbon-based network for efficient electrocatalytic oxygen reduction. *Adv. Mater.* 28, 2337–2344.
37. Zhang, W., Wu, Z.-Y., Jiang, H.-L., and Yu, S.-H. (2014). Nanowire-directed templating synthesis of metal-organic framework nanofibers and their derived porous doped carbon nanofibers for enhanced electrocatalysis. *J. Am. Chem. Soc.* 136, 14385–14388.
38. Lang, X., Hirata, A., Fujita, T., and Chen, M. (2011). Nanoporous metal/oxide hybrid electrodes for electrochemical supercapacitors. *Nat. Nanotechnol.* 6, 232–236.
39. Wang, J., Zhong, H.-X., Qin, Y.-L., and Zhang, X.-B. (2013). An efficient three-dimensional oxygen evolution electrode. *Angew. Chem. Int. Ed.* 52, 5248–5253.
40. Ma, T.Y., Dai, S., Jaroniec, M., and Qiao, S.Z. (2014). Graphitic carbon nitride nanosheet–carbon nanotube three-dimensional porous composites as high-performance oxygen evolution electrocatalysts. *Angew. Chem. Int. Ed.* 53, 7281–7285.
41. Lu, Z., Xu, W., Zhu, W., Yang, Q., Lei, X., Liu, J., Li, Y., Sun, X., and Duan, X. (2014). Three-dimensional NiFe layered double hydroxide film for high-efficiency oxygen evolution reaction. *Chem. Commun.* 50, 6479–6482.
42. Lu, Z., Zhu, W., Yu, X., Zhang, H., Li, Y., Sun, X., Wang, X., Wang, H., Wang, J., Luo, J., et al. (2014). Ultrahigh hydrogen evolution performance of under-water “superaerophobic” MoS<sub>2</sub> nanostructured electrodes. *Adv. Mater.* 26, 2683–2687.
43. Zhao, S., Li, Y., Yin, H., Liu, Z., Luan, E., Zhao, F., Tang, Z., and Liu, S. (2015). Three-dimensional graphene/Pt nanoparticle composites as freestanding anode for enhancing performance of microbial fuel cells. *Sci. Adv.* 1, e1500372.
44. Duan, J., Chen, S., Vasileff, A., and Qiao, S.Z. (2016). Anion and cation modulation in metal compounds for bifunctional overall water splitting. *ACS Nano* 10, 8738–8745.
45. Zhu, Y.P., Ma, T.Y., Jaroniec, M., and Qiao, S.Z. (2017). Self-templating synthesis of hollow Co<sub>3</sub>O<sub>4</sub> microtube arrays for highly efficient water electrolysis. *Angew. Chem. Int. Ed.* 56, 1324–1328.
46. Zhan, W.-W., Kuang, Q., Zhou, J.-Z., Kong, X.-J., Xie, Z.-X., and Zheng, L.-S. (2013). Semiconductor@metal-organic framework core-shell heterostructures: a case of ZnO@ZIF-8 nanorods with selective photoelectrochemical response. *J. Am. Chem. Soc.* 135, 1926–1933.
47. Ma, T.Y., Dai, S., Jaroniec, M., and Qiao, S.Z. (2014). Metal-organic framework derived hybrid Co<sub>3</sub>O<sub>4</sub>-carbon porous nanowire arrays as reversible oxygen evolution electrodes. *J. Am. Chem. Soc.* 136, 13925–13931.
48. Li, Y., Tan, B., and Wu, Y. (2008). Ammonia-evaporation-induced synthetic method for metal (Cu, Zn, Cd, Ni) hydroxide/oxide nanostructures. *Chem. Mater.* 20, 567–576.
49. Jiang, J., Li, Y., Liu, J., Huang, X., Yuan, C., and Lou, X.W. (2012). Recent advances in metal oxide-based electrode architecture design for electrochemical energy storage. *Adv. Mater.* 24, 5166–5180.
50. Liao, J.-Y., Higgins, D., Lui, G., Chabot, V., Xiao, X., and Chen, Z. (2013). Multifunctional TiO<sub>2</sub>-C/MnO<sub>2</sub> core-double-shell nanowire arrays as high-performance 3D electrodes for lithium ion batteries. *Nano Lett.* 13, 5467–5473.
51. Tian, J., Liu, Q., Asiri, A.M., and Sun, X. (2014). Self-supported nanoporous cobalt phosphide nanowire arrays: an efficient 3D hydrogen-evolving cathode over the wide range of pH 0–14. *J. Am. Chem. Soc.* 136, 7587–7590.
52. Zhang, Y., Zhang, W., Yang, Z., Gu, H., Zhu, Q., Yang, S., and Li, M. (2015). Self-sustained cycle of hydrolysis and etching at solution/solid interfaces: a general strategy to prepare metal oxide micro-/nanostructured arrays for high-performance electrodes. *Angew. Chem. Int. Ed.* 54, 3932–3936.
53. Banerjee, R., Phan, A., Wang, B., Knobler, C., Furukawa, H., O’Keeffe, M., and Yaghi, O.M. (2008). High-throughput synthesis of zeolitic imidazolate frameworks and application to CO<sub>2</sub> capture. *Science* 319, 939–943.
54. Chui, S.S.-Y., Lo, S.M.-F., Charmant, J.P.H., Orpen, A.G., and Williams, I.D. (1999). A chemically functionalizable nanoporous material [Cu<sub>3</sub>(TMA)<sub>2</sub>(H<sub>2</sub>O)<sub>3</sub>]. *Science* 283, 1148–1150.
55. Dietzel, P.D.C., Morita, Y., Blom, R., and Fjellvåg, H. (2005). An in situ high-temperature single-crystal investigation of a dehydrated metal-organic framework compound and field-induced magnetization of one-dimensional metal-oxygen chains. *Angew. Chem. Int. Ed.* 44, 6354–6358.
56. Dietzel, P.D.C., Panella, B., Hirscher, M., Blom, R., and Fjellvåg, H. (2006). Hydrogen adsorption in a nickel based coordination polymer with open metal sites in the cylindrical cavities of the desolvated framework. *Chem. Commun.* 42, 959–961.
57. Rosi, N.L., Kim, J., Eddaoudi, M., Chen, B., O’Keeffe, M., and Yaghi, O.M. (2005). Rod packings and metal-organic frameworks constructed from rod-shaped secondary building units. *J. Am. Chem. Soc.* 127, 1504–1518.
58. Zhong, W., Liu, H., Bai, C., Liao, S., and Li, Y. (2015). Base-free oxidation of alcohols to esters at room temperature and atmospheric conditions using nanoscale Co-based catalysts. *ACS Catal.* 5, 1850–1856.
59. Song, F., and Hu, X. (2014). Exfoliation of layered double hydroxides for enhanced oxygen evolution catalysis. *Nat. Commun.* 5, 4477.